Preprint of accepted manuscript in Sensors and Actuators B – Chemical 2018, 261, 135-143. Doi: 10.1016/j.snb.2018.01.145

Stretchable composite monolayer electrodes for low voltage dielectric elastomer actuators

*Xiaobin Ji [a], Alae El Haitami [b], Francesca Sorba [a], Samuel Rosset [a], Giao T.M. Nguyen [b], Cédric Plesse [b], Frédéric Vidal [b], Herbert R. Shea [a] and Sophie Cantin [b]**

[a] Soft Transducers Laboratory (LMTS), École Polytechnique Fédérale de Lausanne (EPFL), Rue de la Maladière 71B, Neuchâtel 2000, Switzerland

[b] Laboratoire de Physicochimie des Polymères et des Interfaces (LPPI, EA2528), Institut des Matériaux, Université de Cergy-Pontoise, 5 mail Gay Lussac 95031 Cergy-Pontoise cedex, France.

ABSTRACT: In this work, a Multiwalled Carbon Nanotube/alkyl-polythiophene (MWCNT/PT) composite was developed as the electrodes for dielectric elastomer actuators (DEAs) using the Langmuir-Schaefer (LS) method. These composites form stable monolayers at the air-water interface that can then be LS transferred onto a Polydimethylsiloxane (PDMS) elastomer membrane. The monolayer electrode remains conductive up to 100% uniaxial strain. We present a method to fabricate DEAs using the LS transferred electrodes. By using a mask during the transfer step, the electrodes can be patterned with better than 200 μm resolution on both sides a 1.4 μm-thick pre-stretched PDMS membrane to produce an ultra-low voltage DEA. The DEA generates 4.0% linear strain at an actuation voltage of 100 V, an order of magnitude lower than the typical DEA operating voltage.

KEYWORDS: Langmuir-Schaefer, low-voltage dielectric elastomer actuator, patterned monolayer electrodes, MWCNT polythiophene composite, large strain actuator, electroactive polymer.

Preprint of accepted manuscript in Sensors and Actuators B – Chemical 2018, 261, 135-143. Doi: 10.1016/j.snb.2018.01.145

1. INTRODUCTION

Soft actuators are required when once wishes to integrate active motion or deformation control in compliant or stretchable objects. Soft actuators are thus used in a broad range of fields where the system must be both soft yet capable of actively changing shape, such as soft robotics,[1,2] tunable optics,[3,4] and compliant grippers.[5,6] Dielectric elastomer actuators (DEAs) are a promising soft actuator technology due to their high energy density,[7] large deformation strain,[8] and fast response.[3] A DEA consists of a dielectric elastomer (DE) (usually silicone[9] or acrylic[7,10]), sandwiched between two compliant electrodes. When a potential difference is applied between the two compliant electrodes, the DE is squeezed in thickness and expands in plane.[7] For deformations of less than approximately 10% (depending on materials and pre-stretch), the in-plane strain S_x is given by[11]:

$$S_x = \varepsilon \frac{E^2}{2Y_m} = \frac{1}{2}\frac{\varepsilon}{Y_m t_m^2} V^2 \quad (1)$$

where ε is the dielectric permittivity of the DE membrane, Y_m the Young's modulus of the DE membrane, E the electric field between the two electrodes, V the applied voltage, and t_m the DE membrane thickness.

The electrodes used for DEAs are generally assumed not to contribute to the stiffness of the devices. This has been the case for many DEAs fabricated using carbon grease electrodes on acrylic films of thickness several tens of μm. The electrode stiffness can only be ignored when the following inequality is respected:[12]

$$Y_e * t_e << Y_m * t_m , \quad (2)$$

where Y_e is the Young's modulus of the electrode, t_e the electrode thickness, Y_m the Young's modulus of the DE, and t_m the DE membrane thickness.

If Eq. 2 is not satisfied (eg, for very thin elastomer membranes, or stiff metallic electrodes), Eq. 1 must be corrected to account for the stiffening impact of the electrodes. This highlights the role of the electrode mechanical properties on the performance of DEAs.

The maximum strain of a DEA is limited by the breakdown field of the DE (more correctly, the failure mode of DEAs is an electromechanical instability[13], but the breakdown field is the key limiting factor for small strain actuator configurations). For typical elastomer thicknesses of 10 μm to 100 μm, and working near typical elastomer breakdown fields of 100 - 150 V/μm, DEAs require from 1 kV to 15 kV to reach maximum strain. These high operating voltages limit some possible applications of DEAs, due to the cost, size, and efficiency of high voltage electronics. Therefore, significant research has been carried out to decrease the DEA operating voltage, while keeping the same actuation performance. As can be seen from Eq. 1, to maintain a given actuation strain while decreasing the voltage, either ε must be increased,[14][ref 9] or Y_m and t_m must be decreased.[15,16] The strain-to-voltage-squared ratio (S_s/V^2) metric has been used to compare the performance of DEAs with different operating voltages.[16] Decreasing the membrane thickness t_m has resulted in the highest previously reported S_s/V^2 value of 125 %/kV^2, for a 3 μm-thick DEA generating 7.5% linear strain at 245 V.[16] Given that the electrodes are generally stiffer than the elastomer ($Y_e > Y_m$ for nearly all materials used in DEAs), when the membrane is made thinner, then the electrode thickness t_e or the electrodes stiffness Y_e must also be further decreased to maintain actuation stain, as summarized in Eq. 2.

Technologies for stretchable electrodes for DEAs, reviewed in references [12,17], include metal ion-implantation,[18] transfer of SWCNT layers,[19] ionogels and hydrogels,[20,21] or silicones or silicone oils doped with carbon black applied by pad printing,[3,16] spray-coating,[10] blade casting [22] or screen-printing.[23] Those electrode fabrication methods are not suitable for DEAs with a membrane thickness of 1 μm, which would allow for DEAs working at 100V, as the electrode thickness is either not negligible with respect to that of the DE membrane, or, for the ion-implanted method, with 50 nm thick electrodes, the electrode stiffness is much too high. A major breakthrough in low-voltage DEAs could be achieved by developing nanometer-thick and stretchable electrodes presenting a low Y_e*t_e value. This would allow the fabrication of DEAs with 1 μm-thick membrane with strain of over 10% at 100 V. To date, electrodes that enable DEAs with more than 1% linear actuation strain under 100 V have not been reported.[16,19,22]

Langmuir technology is an appealing alternative to commonly used electrode fabrication methods as it allows the formation of nm-thick films. It is a powerful tool to transfer molecular monolayers from an air-water interface to a solid substrate. By first spreading and then compressing amphiphilic molecules at the air-water interface, one can fabricate monomolecular films, called Langmuir monolayers, that are highly ordered over areas of several hundreds of cm^2.[24] In addition to producing films one single molecule thick, this technique has the advantage of controlling the density of molecules in the monolayer. These Langmuir monolayers can then be transferred to a chosen substrate using the vertical Langmuir-Blodgett (LB) or horizontal Langmuir-Schaefer (LS) method.[25] Several devices including molecular sensors,[26] photo-electrochemical devices,[27] organic semi-conductor devices,[28] and field effect transistors,[29] have been fabricated using Langmuir technology. DEA electrodes based on stretchable monolayer conductors fabricated by the Langmuir technology have not yet been reported.

In this article, Langmuir technology was used to fabricate stretchable monolayer electrodes for DEAs (Fig. 1). Hydrophobic alkyl-polythiophenes (PT) and hydrophilic Multiwalled Carbon Nanotubes (MWCNT) were mixed in a solvent to form a stable amphiphilic composite dispersion. This dispersion was spread on the water surface to form a composite monolayer electrode, in which the MWCNT network was embedded in a PT monolayer (Fig. 1a). PT, as conducting polymer, should contribute to the electronic conductivity and stabilize non-functionalized hydrophilic MWCNT at the air-water interface. Two types of PT with different linear alkyl side chains (poly-3-hexylthiophene (P3HT) and poly-3-decylthiophene (P3DT)) were studied, since it was shown that the side chain length has a significant effect on the bulk material properties. The longer this chain is (up to 12 C), the smaller the Young's modulus and the electrical conductivity.[30] The MWCNT/PT composite monolayer was then transferred from the air-water interface to polydimethylsiloxane (PDMS) elastomer membrane using the LS method (Fig. 1b). The adhesion was provided by the hydrophobic affinity between the PDMS substrate and PT from the composite monolayer. The 1.4 μm-thick pre-stretched PDMS membrane was sandwiched between two LS transferred composite electrodes to make a 100 V operating DEA (Fig. 1c). The electrodes were evaluated based on their morphological, electrical and mechanical properties with regards to DEA application.

2. EXPERIMENTAL SECTION

2.1 Chemicals

Regio-regular poly(-3-hexyl-thiophene-2,5-diyl) (P3HT, CAS 156074-98-5 and purity of 99.995%), and regio-regular poly(-3-decyl-thiophene-2,5-diyl) (P3DT, CAS 110851-65-5 and purity of 99.995%) were ordered from Sigma-Aldrich and used as received. Multiwalled Carbon Nanotubes (MWCNTs; external diameter 15-35 nm, length ≥ 10 μm) were purchased from Nanothinx S.A. (Rio, Greece). Poly(acrylic acid) (PAA, 25% soln. in water, CAS 9003-01-4) was ordered from

Chemie Brunschwig. Ethanol (99.9%) and chloroform (99.2%) were ordered from VWR Prolabo Chemicals. PDMS (Sylgard 186, MED-4086) and PDMS solvent (OS-2) were ordered from Dow Corning (Auburn, MI).

2.2 Fabrication of DEA electrodes using LS method

2.2.1 Polythiophene (PT) solutions. PT (P3DT or P3HT) solution (0.167 g/L) was prepared in chloroform-ethanol 9:1 v/v and then sonicated for 30 min.

2.2.2 MWCNT/PT mixed solutions. PT was dissolved in a chloroform solution (0.167 g/L), then sonicated for 30 min. MWCNTs were dispersed in ethanol (20 g/L), then sonicated for 1 h. Both solutions were mixed in a volume fraction of 9 (chloroform)/ 1 (ethanol) and then sonicated for 5 h before being centrifuged for 15 min at 3000 rpm. The supernatant was collected and two additional centrifugations of 15 min each were performed. This process was optimized according to the optical microscopy images and the surface resistance value of the LS transferred composite MWCNT/PT monolayers as outlined in the supplementary data (section 1, Fig. S1 and Table S1).

2.2.3 Monolayer electrode fabrication. The monolayers were formed in a KIBRON Langmuir-Blodgett (LB) trough (MicroTroughX). An adequate solution volume was spread over an ultrapure water surface (18.2 MΩ • cm Millipore Simplicity, Billerica, MA) using a micro syringe. After solvent evaporation, the monolayer was compressed at a barrier speed of 10 mm/min and the surface pressure recorded. In the following, the isotherms are presented as a function of the trough area instead of the area per monomer. The monolayer homogeneity at the air-water interface was verified in-situ by Brewster Angle Microscopy; more detail on this technique is given in the supplementary data (section 2). [31] For the LS transfer, the monolayer was kept at a surface pressure of 15 mN/m and the PDMS substrate was horizontally moved towards the monolayer at 2 mm/min using a stepper

motor from KIBRON. Once substrate/monolayer contact was established, the PDMS substrate was raised until the transfer was complete.

2.3 Atomic Force Microscopy (AFM). 100 μm-thick PDMS membranes were fabricated using the method reported by Rosset et al, [32] and used as substrates for the LS transfer of the monolayer electrode (Supplementary data, section 3.1). The AFM images were performed using the Peak Force Tapping mode with a Dimension ICON microscope from Brüker. AFM imaging was carried out in air using ScanAsyst-air cantilevers (Brüker) with a spring constant of 0.4 $N.m^{-1}$. 10 µm x 10 µm images were obtained with the height mode and a 256 x 256 resolution, at a 0.5 Hz scan rate. Data processing was performed with NanoScope software version 1.40 (Brüker).

2.4 Surface resistance measurement. The monolayers LS transferred onto PDMS substrates were placed against two rectangular copper electrodes enclosing a 1cm x 1cm square as active zone. The resistance was determined from the measured current with 10 V applied between the copper electrodes. A Gamry Instruments potentiostat (reference 600) was used for these measurements.

2.4.1 Surface resistance stability as function of time. The effect of polythiophene doping on the surface resistance stability was investigated. The transferred PT monolayers were immersed into a 0.15M $FeCl_3$ acetonitrile solution for 5 min and then rinsed with acetonitrile [29]. For each type of monolayer, six individual samples were measured to obtain an average value and standard deviation.

2.4.2 Surface resistance as function of strain. The surface resistance of monolayers LS transferred onto suspended 100 μm-thick PDMS substrates was measured for different stretching conditions. Two samples were used in each case and a speed of 1 % lengthening/s was applied during stretching. The effect of sample cycling on the surface resistance was also investigated. Fort that, 10 stretch-release cycles (1 %/s) per sample were used, with 30 s delay between each cycle.

2.5 Young's modulus measurement of monolayers

The Young's modulus of the monolayer electrode was measured by Pull test using a uniaxial tensile testing setup. By measuring the stiffening impact of the monolayer on a very soft PDMS substrate (Young's modulus of 40 kPa), the Young's modulus of the monolayer could be computed (more details on the PDMS preparation are given in supplementary data, section 3.2). Uniaxial cyclic stretching (20% strain) was applied to the PDMS membrane using a linear motor (UAL from Saia-Burgess) at a strain rate of 0.67 %/s. The stretching direction was parallel to the 2 mm edge of the PDMS rectangle so that stretched PDMS membrane was in a pure shear stress state. During the measurement, the force and the sample elongation were simultaneously measured using a force sensor (Futek LSB200, capacity 100 mN) and the encoder of the stepper motor, thus enabling the representation of the stress-strain relationship. A LabVIEW code was written to control the motor and the force sensor for the whole experiment process.

After measuring the Young's modulus of bare PDMS membranes, the monolayer electrodes were LS transferred on those PDMS membranes. The Young's modulus of the PDMS + electrode bilayer was determined using the same parameters as for the bare PDMS membrane. The PDMS + electrode bilayer was formed by two adherent layers with equal length and width, so the electrode Young's modulus was calculated using [33]:

$$Y_{bilayer}t_{bilayer} = Y_{PDMS}t_{PDMS} + Y_{electrode}t_{electrode}\ , \qquad (3)$$

where Y is the Young's modulus and t the thickness.

2.6 DEAs fabrication

A 2.0 μm-thick PDMS membrane (Sylgard 186, Dow Corning) was prepared as the DE membrane of the DEA (details on the PDMS membrane fabrication are given in supplementary data, section

3.3). To handle and pre-stretch sub-micrometer suspended PDMS membranes, a stretchable holder was developed, made from acrylic adhesive (3M, VHB 4905) covered with silicone transfer adhesive (Adhesive Research, ARclear 8932). Using the stretchable holder, a suspended 2.0 μm-thick PDMS membrane was released from the PET substrate, and pre-stretched equi-biaxially to 1.4 μm-thick with a linear ratio of 1.2 (Fig. 2a). The pre-stretched PDMS was fixed onto a Poly(methyl methacrylate) (PMMA) holder (Fig. 2b). A mask (made from the backing film of the silicon adhesive, ARclear 8932) was placed on the suspended PDMS (Fig. 2c). The mask serves to pattern the monolayer by LS transfer and to keep the suspended PDMS membrane flat (Fig. 2d). After the LS transfer of monolayer electrode, one drop of ethanol was deposited between the gap of the mask and the PDMS layer to help in peeling off the mask. The thin pre-stretched PDMS membrane with patterned monolayer electrode on one side was obtained (Fig. 2e). To LS transfer the monolayer electrode on the other side of the same PDMS membrane, a smaller holder with copper connections was used (Fig. 2f). On this smaller holder, the first patterned electrode was in contact with the copper connection (Fig. 2g), and the second electrode was LS transferred on the other side (Fig. 2c-2e). Another smaller holding ring was bonded to the DEA to provide the electrical contact for the second electrode (Fig. 2h). A small drop of conductive silver epoxy was used to ensure a good electrical connection between the monolayer electrode and the copper tape (See supplementary information, section 4, Fig S3). The active zone of the DEA (3 mm diameter cycle) was located at the center of the pre-stretched 1.4 μm-thick PDMS membrane, where the two electrodes overlap.

Voltages up to 130 V were applied between the two electrodes of the fabricated DEA. The diameter linear strain of the center active zone was measured as a function of the applied voltage. The linear strain was also measured as a function of frequency to characterize the speed of the DEA.

3. RESULTS AND DISCUSSION

3.1 Monolayer electrode properties

In the two following sections, electrodes based on MWCNT/P3HT and MWCNT/P3DT monolayers transferred onto PDMS substrate were characterized regarding structure, surface morphology, surface resistance and Young's modulus.

3.1.1 Characterization of the monolayer electrode

The MWCNT/PT monolayer properties were first investigated at the air-water interface. The monolayers were then transferred onto PDMS substrates and their morphology was characterized by AFM. Surrface resistance was measured vs. time.

3.1.1.1 Monolayer structure at the air-water interface and onto PDMS substrate

Compression isotherms of the two MWCNT/P3DT and MWCNT/P3HT composite monolayers spread at the air-water interface are shown in Fig. 3a. The isotherms for both systems have similar shapes, characterized by a steep rise in surface pressure until collapse is detected at around 60 mN/m. This indicates the formation of condensed and stable monolayers at the air-water interface. It should be noted that in the absence of PT, MWCNTs do not form a Langmuir monolayer at the air-water interface. A Brewster Angle Microscopy (BAM) image of the MWCNT/P3DT monolayer compressed at 15 mN/m is shown as inset in Fig. 3a. By comparison with the pure PT monolayer (Supplementary data, section 2, Fig. S2), MWCNTs embedded in the PT condensed phase can be observed as small brighter spots with a size of a few microns. Some slightly larger bright spots corresponding to MWCNT aggregates can also be observed. Similar behavior is observed for the MWCNT/P3HT monolayer. BAM images thus confirm that PTs are good dispersants for MWCNT.[34] To gain further insight in the structure of this monolayer, AFM images were taken of the monolayers transferred onto 100 μm-thick PDMS substrates at a surface pressure of 15 mN/m

(Fig. 3b). As no significant effect of the PT side chain length was detected, only the AFM image of the MWCNT/P3DT system is shown. AFM topography reveals a uniform and dense MWCNT carpet. MWCNTs are clearly interconnected forming a network which reflects the successful LS transfer of the composite monolayer from the water surface to the PDMS substrate.

The electrode thickness was obtained from AFM height profiles on a MWCNT/P3DT monolayer electrode transferred onto a smooth glass substrate. The MWCNT network presents an average thickness of about 30 nm, which corresponds to the expected diameter of the MWCNT. As the very thin P3DT continuous phase is not easily detected on these height profiles, its thickness of 2 nm was obtained from LS transferred pure P3DT monolayers. The thickness of the composite monolayer electrode thus varies between 2 nm and 30 nm, according to the thickness of both components (Supplementary data, section 5, Fig. S4).

3.1.1.2 Monolayer electrode surface resistance : stability over time

Because doping of electronically conducting polymers can strongly increase their electronic conductivity,[29] the surface resistance of doped and undoped pure P3DT monolayers (see Section 2.2) was compared. The role of MWCNTs within the MWCNT/P3DT composite monolayer was then highlighted by comparison with pure P3DT monolayer.

The change in surface resistance as function of time is shown in Fig. 4 for undoped and doped P3DT monolayers (with no CNTs). The surface resistance of doped P3DT monolayer presents an acceptable value for DEAs of about 20MΩ/□ immediately after doping. However, the resistance increases with time due to a progressive de-doping process, reaching a high and stable value of 80 GΩ/□ after 24 h. Since the electrode conductivity must remain stable for DEA applications, this electrode based on a doped P3DT monolayer cannot be used. The undoped P3DT monolayer has an initial surface resistance of order GΩ/□, increases by about one order of magnitude after a few hours,

and finally reaches a stable high value (~ 50 GΩ/□) after 24 h. Thus, as the doped P3DT monolayer, the undoped P3DT monolayer cannot be used as an electrode for DEAs.

For the composite monolayer consisting of undoped P3DT and MWCNTs, an initial surface resistance of about 20 MΩ/□ is measured, two order of magnitude lower than that of undoped P3DT. This value is close to the one measured for freshly doped P3DT, however the surface resistance stability is greatly improved by the presence of MWCNTs, remaining stable even after 48 h (Fig. 4). This result indicates that in the presence of undoped P3DT, the electronic properties of the composite monolayer are dominated by MWCNTs.

The surface resistance as a function of time for the undoped MWCNT/P3HT electrode is independent of the PT side chain length (Supplementary data, section 6, Fig. S5). Electrodes with both PTs present a stable surface resistance for 48 h, with almost similar values (~ 40MΩ/□). While side chain length of PT usually has a significant effect on electronic properties of bulk material, [30] no effect is observed here since the electronic properties of the composite monolayers are mainly governed by the MWCNT network.

The surface resistance of the both MWCNT/PT composite monolayers have values that are acceptable for DEAs .[17] The DEA must be evaluated in terms as its charging time, ie RC time constant (see section 3.2.).

3.1.2 Influence of different stretching conditions

Because the surface resistance and topography are very similar for both MWCNT/P3HT and MWCNT/P3DT systems, the electrode characterizations performed under different stretching conditions were carried out only on MWCNT/P3DT monolayers. The morphology of the MWCNT/P3DT composite monolayer for different stretching conditions was investigated. The

surface resistance as a function of strain was then characterized. Finally, the electrode Young's modulus was measured.

3.1.2.1 Morphology of MWCNT/P3DT electrode under different PDMS membrane stretching conditions

To study the possible changes in surface topography upon stretching of the 100 μm-thick PDMS substrate covered by the MWCNT/P3DT electrode, AFM images were taken under different stretching conditions (Fig. 5 and Supplementary data, section 7, Fig. S6).

From Fig. 5a, taken at 20% uniaxial strain applied to the PDMS substrate, one can see that the MWCNTs are slightly deformed along the stretching direction, but remain interconnected. For device at 0% strain, taken after 100% uniaxial strain (Fig. 5b) or after 10 cycles with 60% uniaxial strain (Fig. 5c), AFM images show an interconnected MWCNT network, indicating that stretching up to 100% does not break the network. For all stretching conditions, no significant morphology change is detected at this length scale once the sample is relaxed back to 0 % strain (Fig. 5d).

3.1.2.2 Influence of the applied strain on the electrode surface resistance

The evolution of the surface resistance of the MWCNT/P3DT composite monolayer as a function of the applied strain is shown in Fig. 6, based on two samples (see Section 2.4).

Fig. 6a shows the change of the surface resistance for a sample submitted to different successive cycles of increased maximum strain between 20% and 100%. Only the stretching up cycles are presented. During the first 20% strain, the resistance increases by about one order of magnitude, indicating a decrease in the interconnection ratio within the MWCNT network. When returning to 0% strain, the resistance does not reach its the initial value, but increased by a factor of 6. This highlights an irreversible change in electrical properties due to mechanical deformation. This occurs

on every cycle with increasing maximum applied strain. One can however observe that the increase in surface resistance after returning to 0% strain is less pronounced above 60% strain. It is noteworthy that the monolayer electrode remains conductive up to 100 % uniaxial strain.

In order to understand whether this change in resistance is related to cycle number or to the maximum strain, another sample was stretched repeatedly to a constant maximum strain of 60%. The surface resistance variation through each of the 10 stretch cycles is shown in Fig. 6b. One should mention that the end points of both up and down cycles do not present exactly the same value, which is due to the 30 s delay during the measurement. Upon the first cycle, the surface resistance increases by about one order of magnitude reaching ~ 317 MΩ/□ as the strain varies from 0% to 60%. One can observe that this variation is lower than the one obtained at 60% strain for the sample considered in Fig. 6a, due to the different history that both samples have experienced. One can also notice that the main evolution is observed during the first 40% strain. After returning to 0% strain, as previously evidenced, the surface resistance does not recover its value before stretching, meaning that the MWCNT network interconnection is changed irreversibly. For the 9 other following cycles to 60 % linear strain, the surface resistance does not change drastically. Thus, even though monolayer electrical properties degradation occurs during the first stretch cycle, the sample can be submitted to many successive cycles at quite large strain without significant variation of electrode surface resistance. By comparing Fig. 6a and 6b, it can be concluded that the degradation of the monolayer electrode is mainly related to the maximum applied strain.

3.1.2.3 Electrode Young's modulus

An example of stress-strain curves is shown in Fig. 7 for both the 10 μm-thick bare PDMS substrate and the bilayer consisting of the same PDMS substrate covered by the MWCNT/P3DT monolayer electrode. Young's moduli of 34.1 kPa and 40.8 kPa are extracted for the bare PDMS substrate and

the PDMS/electrode bilayer respectively. A $Y_{electrode}*t_{electrode}$ value of 0.08 ± 0.03 N/m is then deduced from Eq. 3. Since the composite monolayer consists of a 30nm-thick interconnected MWCNT network embedded inside a 2 nm-thick P3DT monolayer (Section 3.1.1.1.), the Young's modulus of the electrode $Y_{electrode}$ can then be computed as being between 3 ± 1 and 37 ± 14 MPa, depending what electrode thickness is used.

The Young's modulus of pure P3DT monolayers was also measured for comparison. A $Y_{PT}*t_{PT}$ value of 0.07 ± 0.03 N/m is obtained, leading to a Y_{PT} value of 37 ± 16 MPa using 2 nm as electrode thickness. For both pure P3DT and MWCNT/ P3DT monolayers, nearly the same $Y*t$ value is obtained. Therefore, it can be deduced that within the composite monolayer, the P3DT continuous phase plays the dominating role for the Young's modulus. The presence of the MWCNT network embedded inside the P3DT monolayer does not increase the stiffness of the monolayer.

The composite MWCNT/ P3DT monolayer electrodes have a surface resistance of about 20 MΩ/□, remain conductive at 100% linear strain, and show a small Y_e*t_e product (0.08 N/m) in comparison with the $Y_{PMDS}*t_{PDMS}$ product of the 1.4 μm thick PDMS membrane used in the ultrathin DEA (1MPa x $1.4.10^{-6}$ m = 1.4 N/m). All these properties lead to a promising electrode material to fabricate a low voltage operating DEA.

3.2 100 V operating DEA with stretchable MWCNT/P3DT monolayer electrodes

A Dielectric Elastomer Actuator was fabricated by patterning the stretchable MWCNT/P3DT composite monolayer electrodes on both sides of a 1.4 μm-thick suspended pre-stretched PDMS membrane (see section 2.6). Prior to our work, one important factor limiting strain in extremely thin DEAs was the stiffening impact of the electrodes.[16] The MWCNT/P3DT monolayer electrodes add very little stiffness to the DEA, allowing good strain at 100V, but such thin electrodes have

higher resistivity, limiting device speed. We thus report here both strain and speed data for our DEAs.

The linear strain of the fabricated DEA active zone is plotted as a function of the applied voltage in Fig. 8a. This device is the thinnest DEA reported to date. For the first time, DEA actuation strains of well above 1% are obtained with driving voltages below 100 V. 4.0% linear strain is obtained for a 100V driving voltage, which corresponds to a S/V^2 value of 400 %/kV^2. This value is three times higher than the one reported by Poulin et al, [16]. The strain vs. true electric field is shown in Supplementary data (section 8, Figure S7). Despite the very thin elastomer, the curve matches well our typical data for thicker Sylgard 186 membranes.

The actuation strain vs. actuation frequency curve was recorded, as shown in Fig. 8b. For frequencies below approximately 0.2 Hz, the strain is constant, and for higher frequencies the strain decreases. The electromechanical 3dB point occurs at 1 Hz. Two main reasons can lead to this response speed: electrical charging time, and visco-elastic losses.

The electrical charging time of a DEA can be also approximated as RC, where R is the total resistance of the electrodes (including feedlines) and C is the capacitance of the DEA. At 100 V (i.e., at 4% strain), the total resistance of the 2 electrodes is 860 MΩ, and the capacitance of the DEA is calculated as 1.4 x 10^{-10} F. The computed RC time constant is 120 ms.

The charging time constant of the DEA was determined experimentally by recording the current flowing to the DEA in response to a step in drive voltage. The classical current jump followed by an exponential decay was observed, from which an electrical charging time constant τ of 150 ms was extracted. In the highly simplified model of an RC circuit, the RC time constant corresponds to the time at which the voltage reaches 63.2% of its maximum value. Given the quadratic response

of DEAs, 63% of the voltage corresponds to 40% of the maximum strain. Using 100V as our drive voltage, one sees in Figure 8a that the linear strain at 63 V is 1.5%. From the strain vs charging time plot at 100V (see Supplementary data, section 8, Fig S8), 1.5% linear strain is reached between 125 ms and 250 ms, consistent with the electrical charging time.

The overall response speed can thus be mostly explained by the electrical charging time constant. The response time has also a small component due the visco-elastic response of the elastomer. We expect the later to be very small, given our prior experience with kHz DEAs using similar silicone elastomers [3].

4 CONCLUSIONS

The Langmuir-Schaefer method was used for the first time here to fabricate ultra-thin stretchable electrodes for dielectric elastomer actuators. Multiwalled Carbon Nanotube and alkyl-polythiophene were combined to form stable monolayers at the air-water interface that were transferred onto a PDMS membrane using the Langmuir-Schaefer technology. The monolayer electrode consists of an interconnected MWCNT network embedded in a PT monolayer, in which the PT imparts the mechanical properties while the MWCNTs ensure the electrical conductivity of the system. The composite monolayer is stretchable, and conductive up to 100% strain (~ 20 MΩ/□ at 0% strain, ~ 5 GΩ/□ at 100% strain). Using the LS method to fabricate patterned ultrathin stretchable electrodes enables the fabrication of a thin DEA with a 1.4 μm-thick PDMS dielectric membrane. At only 100 V, this DEA reaches 4.0% linear strain. Compared to the kV driving voltage generally required for DEAs, this low operating voltage opens new applications for DEAs.. The LS electrodes that we report here are a key building block towards DEAs generating full strain at less than 5 V: by using LS/LB techniques to make both the elastomer and the electrodes, it will be possible to make

multilayer DEAs where all layers are one single molecule thick. This will be the ultimate physical limit in DEA technology.

AUTHOR INFORMATION

Corresponding Author

*E-mail: sophie.cantin-riviere@u-cergy.fr

ACKNOWLEDGMENT

We gratefully acknowledge Dr. Jun Shintake, Dr. Matthias Imboden, Dr. Alexandre Poulin and Mr. Samuel Schlatter for their hopeful comments and discussion. This work was funded by the European Union's Horizon 2020 research and innovation programme under the Marie Skłodowska-Curie grant agreement No 641822—MICACT via the Swiss State Secretariat for Education, Research, and Innovation.

REFERENCES

[1] D. Rus, M.T. Tolley, Design, fabrication and control of soft robots, Nature. 521 (2015) 467–475. doi:10.1038/nature14543.

[2] M. Wehner, R.L. Truby, D.J. Fitzgerald, B. Mosadegh, G.M. Whitesides, J.A. Lewis, R.J. Wood, An integrated design and fabrication strategy for entirely soft, autonomous robots, Nature. 536 (2016) 451–455. doi:10.1038/nature19100.

[3] L. Maffli, S. Rosset, M. Ghilardi, F. Carpi, H. Shea, Ultrafast all-polymer electrically tunable silicone lenses, Advanced Functional Materials. 25 (2015) 1656–1665. doi:10.1002/adfm.201403942.

[4] S. Shian, R.M. Diebold, D.R. Clarke, Tunable lenses using transparent dielectric elastomer actuators., Optics Express. 21 (2013) 8669–76. doi:10.1364/OE.21.008669.

[5] F. Ilievski, A.D. Mazzeo, R.F. Shepherd, X. Chen, G.M. Whitesides, Soft robotics for chemists, Angewandte Chemie - International Edition. 50 (2011) 1890–1895. doi:10.1002/anie.201006464.

[6] J. Shintake, S. Rosset, B. Schubert, D. Floreano, H. Shea, Versatile Soft Grippers with Intrinsic Electroadhesion Based on Multifunctional Polymer Actuators, Advanced Materials. 28 (2016) 231–238. doi:10.1002/adma.201504264.

[7] R. Pelrine, R. Kornbluh, Q. Pei, J. Joseph, High-speed electrically actuated elastomers with strain greater than 100%, Science (New York, N.Y.). 287 (2000) 836–9.

doi:10.1126/science.287.5454.836.
[8] C. Keplinger, T. Li, R. Baumgartner, Z. Suo, S. Bauer, Harnessing snap-through instability in soft dielectrics to achieve giant voltage-triggered deformation, Soft Matter. 8 (2012) 285–288. doi:10.1039/C1SM06736B.
[9] F.B. Madsen, A.E. Daugaard, S. Hvilsted, A.L. Skov, The Current State of Silicone-Based Dieletric Elastomer Transducers, Macromolecular Rapid Communications. 37 (2016) 378–413.
[10] W. Yuan, L. Hu, Z. Yu, T. Lam, J. Biggs, S.M. Ha, D. Xi, B. Chen, M.K. Senesky, G. Grüner, Q. Pei, Fault-tolerant dielectric elastomer actuators using single-walled carbon nanotube electrodes, Advanced Materials. 20 (2008) 621–625. doi:10.1002/adma.200701018.
[11] R.E. Pelrine, R.D. Kornbluh, J.P. Joseph, Electrostriction of polymer dielectrics with compliant electrodes as a means of actuation, Sensors and Actuators A: Physical. 64 (1998) 77–85. doi:10.1016/S0924-4247(97)01657-9.
[12] D. McCoul, W. Hu, M. Gao, V. Mehta, Q. Pei, Recent Advances in Stretchable and Transparent Electronic Materials, Advanced Electronic Materials. 2 (2016) 1500407. doi:10.1002/aelm.201500407.
[13] S.J.A. Koh, T. Li, J. Zhou, X. Zhao, W. Hong, J. Zhu, Z. Suo, Mechanisms of large actuation strain in dielectric elastomers, Journal of Polymer Science, Part B: Polymer Physics. 49 (2011) 504–515. doi:10.1002/polb.22223.
[14] S.J. Dünki, Y.S. Ko, F.A. Nüesch, D.M. Opris, Self-repairable, high permittivity dielectric elastomers with large actuation strains at low electric fields, Advanced Functional Materials. 25 (2015) 2467–2475. doi:10.1002/adfm.201500077.
[15] M. V. Circu, Y.S. Ko, A.C. Gerecke, D.M. Opris, Soft polydimethylsiloxane thin elastomeric films by in situ polymerization to be used as dielectricum in actuators, Macromolecular Materials and Engineering. 299 (2014) 1126–1133. doi:10.1002/mame.201300457.
[16] A. Poulin, S. Rosset, H.R. Shea, Printing low-voltage dielectric elastomer actuators, Applied Physics Letters. 107 (2015). doi:10.1063/1.4937735.
[17] S. Rosset, H.R. Shea, Flexible and stretchable electrodes for dielectric elastomer actuators, Applied Physics A: Materials Science and Processing. 110 (2013) 281–307. doi:10.1007/s00339-012-7402-8.
[18] S. Rosset, M. Niklaus, P. Dubois, H.R. Shea, Large-stroke dielectric elastomer actuators with ion-implanted electrodes, Journal of Microelectromechanical Systems. 18 (2009) 1300–1308. doi:10.1109/JMEMS.2009.2031690.
[19] M. Duduta, R.J. Wood, D.R. Clarke, Multilayer Dielectric Elastomers for Fast, Programmable Actuation without Prestretch, Advanced Materials. 28 (2016) 8058–8063. doi:10.1002/adma.201601842.
[20] C. Keplinger, J.-Y. Sun, C.C. Foo, P. Rothemund, G.M. Whitesides, Z. Suo, Stretchable, Transparent, Ionic Conductors, Science. 341 (2013) 984–987. doi:10.1126/science.1240228.
[21] B. Chen, Y. Bai, F. Xiang, J.Y. Sun, Y. Mei Chen, H. Wang, J. Zhou, Z. Suo, Stretchable and transparent hydrogels as soft conductors for dielectric elastomer actuators, Journal of Polymer Science, Part B: Polymer Physics. 52 (2014) 1055–1060. doi:10.1002/polb.23529.
[22] O.A. Araromi, S. Rosset, H.R. Shea, High-Resolution, Large-Area Fabrication of Compliant Electrodes via Laser Ablation for Robust, Stretchable Dielectric Elastomer Actuators and Sensors, ACS Applied Materials & Interfaces. 7 (2015) 18046–18053. doi:10.1021/acsami.5b04975.
[23] B. Fasolt, M. Hodgins, G. Rizzello, S. Seelecke, Effect of screen printing parameters on sensor and actuator performance of dielectric elastomer (DE) membranes, Sensors and

Actuators, A: Physical. 265 (2017) 10–19. doi:10.1016/j.sna.2017.08.028.

[24] A. El Haitami, E.H.G. Backus, S. Cantin, Synthesis at the Air–Water Interface of a Two-Dimensional Semi-Interpenetrating Network Based on Poly(dimethylsiloxane) and Cellulose Acetate Butyrate, Langmuir. 30 (2014) 11919–11927. doi:10.1021/la502514e.

[25] G.L. Gaines, Insoluble monolayers at liquid-gas interfaces, Interscience Publishers, New York, 1966. https://searchworks.stanford.edu/view/699189 (accessed July 3, 2017).

[26] A.R. Tao, F. Kim, C. Hess, J. Goldberger, R. He, Y. Sun, Y. Xia, P. Yang, Langmuir–Blodgett Silver Nanowire Monolayers for Molecular Sensing Using Surface-Enhanced Raman Spectroscopy, Nano Letters. 3 (2003) 1229–1233. doi:10.1021/nl0344209.

[27] V. Sgobba, G. Giancane, D. Cannoletta, A. Operamolla, O. Hassan Omar, G.M. Farinola, D.M. Guldi, L. Valli, Langmuir-schaefer films for aligned carbon nanotubes functionalized with a conjugate polymer and photoelectrochemical response enhancement, ACS Applied Materials and Interfaces. 6 (2014) 153–158. doi:10.1021/am403656k.

[28] L. Huang, X. Hu, L. Chi, Monolayer-Mediated Growth of Organic Semiconductor Films with Improved Device Performance, Langmuir. 31 (2015) 9748–9761. doi:10.1021/acs.langmuir.5b00349.

[29] J. Matsui, S. Yoshida, T. Mikayama, A. Aoki, T. Miyashita, Fabrication of polymer Langmuir-Blodgett films containing regioregular poly(3-hexylthiophene) for application to field-effect transistor, Langmuir. 21 (2005) 5343–5348. doi:10.1021/la046922n.

[30] J. Moulton, P. Smith, Electrical and mechanical properties of oriented poly (3-alkylthiophenes): 2. Effect of side-chain length, Polymer. 33 (1992) 2340–2347.

[31] S. Hénon, J. Meunier, Microscope at the Brewster angle: Direct observation of first-order phase transitions in monolayers, Review of Scientific Instruments. 62 (1991) 936–939. doi:10.1063/1.1142032.

[32] S. Rosset, O.A. Araromi, S. Schlatter, H.R. Shea, Fabrication Process of Silicone-based Dielectric Elastomer Actuators, Journal of Visualized Experiments. (2016) e53423–e53423. doi:10.3791/53423.

[33] I.M. (Ian M. Ward, J. (John) Sweeney, An introduction to the mechanical properties of solid polymers, Wiley, 2004.

[34] C. Lo, Y. Lee, W. Hsu, Behavior of mixed multi-walled carbon nanotube / P3HT monolayer at the air / water interface, Synthetic Metals. 160 (2010) 2219–2223. doi:10.1016/j.synthmet.2010.08.014.

- FIGURES

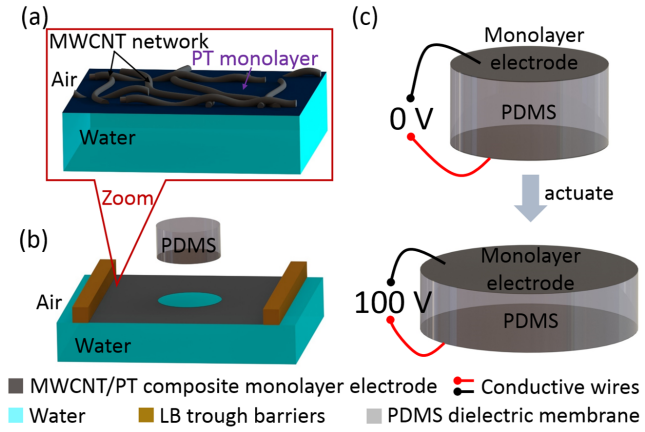

Fig. 1. Low-voltage DEAs made using Langmuir-Schaefer transferred monolayer electrodes (a) Monolayer composite electrode formed at the air-water interface: interconnected MWCNT network embedded inside an alkyl-polythiophene (PT) monolayer. (b) Langmuir-Schaefer (LS) transfer of the composite monolayer from the air-water interface onto the PDMS dielectric membrane to make one electrode of the DEA. (c) The DEA consists of a 1.4 µm-thick silicone membrane sandwiched between two sub-100nm thick composite monolayer electrodes.

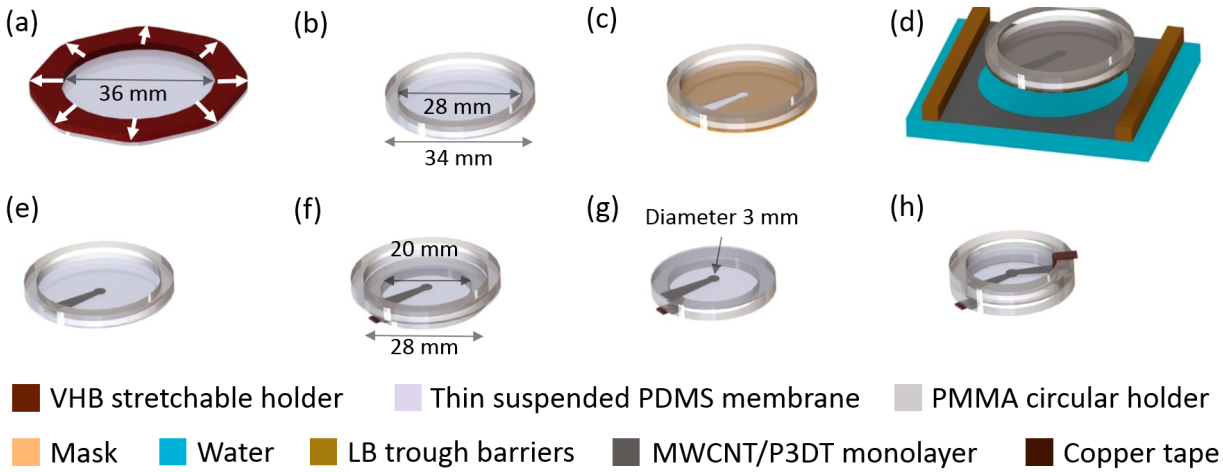

Fig. 2. Fabrication process of 1.4 µm-thick DEA by using LS technology. (a) Suspended PDMS (Sylgard 186) equi-biaxially pre-stretched (initial thickness: 2.0 µm, after stretch: 1.4 µm). (b) Suspended stretched 1.4 µm-thick PDMS membrane fixed onto a PMMA holder. (c) A mask is placed on the suspended membrane. (d) LS transfer of the monolayer electrode formed at the air-water interface onto the suspended PDMS membrane with mask. (e) Patterned monolayer electrode on the PDMS. (f) Transferring the PDMS membrane covered with the patterned monolayer electrode onto a smaller PMMA holder. (g) Patterned monolayer electrode on the lower side of PDMS with the electrode connected with copper tape, and the upper side of PDMS without electrode. (h) DEA made with LS electrode technology.

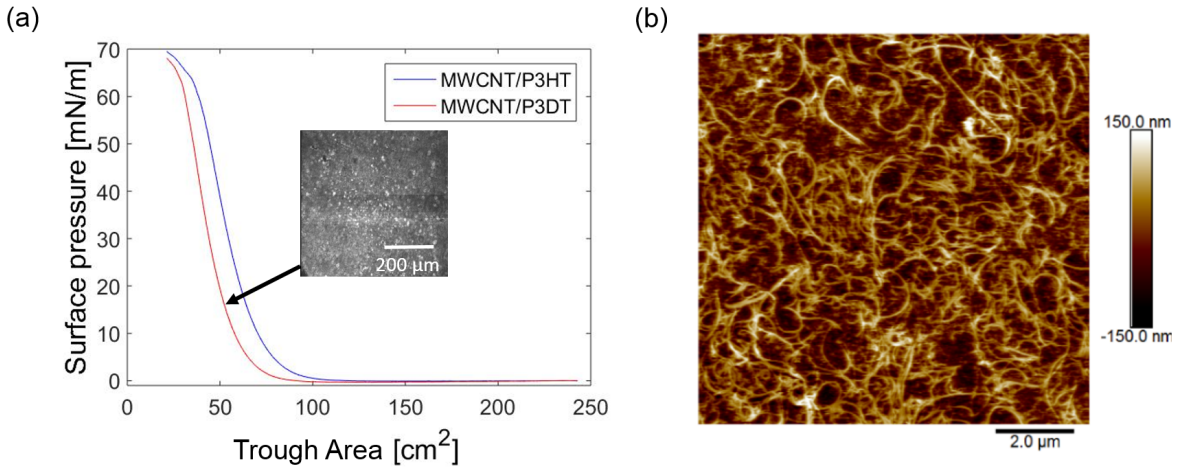

Fig. 3. (a) Surface pressure versus trough area isotherms for MWCNT/P3HT and MWCNT/P3DT monolayers with BAM images of MWCNT/P3DT monolayer at 15 mN/m. (b) AFM image of MWCNT/P3DT monolayer transferred at 15 mN/m onto PDMS substrate.

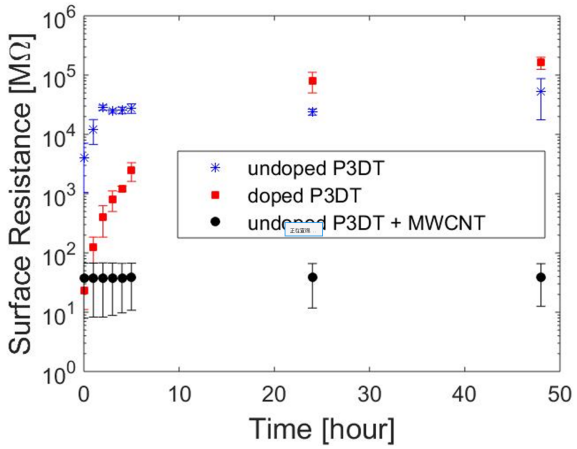

Fig. 4. Surface resistance of undoped MWCNT/ P3DT and MWCNT/ P3HT composite monolayer electrodes as a function of time.

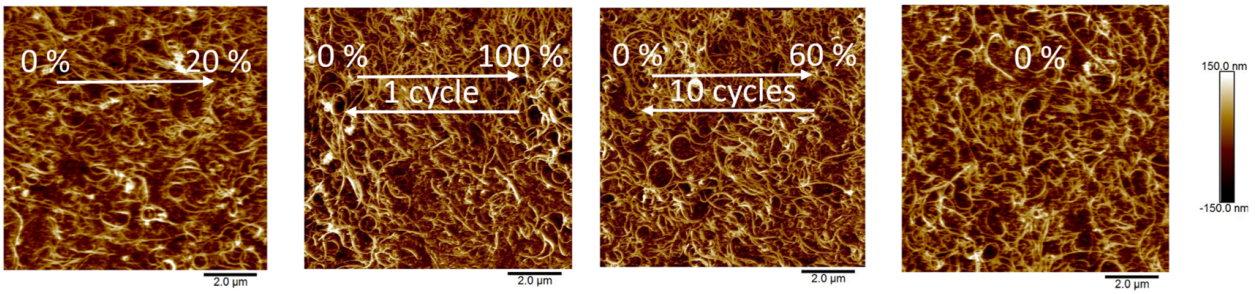

Fig. 5. AFM images of MWCNT/P3DT monolayer electrode. (a) At 20% uniaxial strain. (b) Returning to 0% strain after 100% uniaxial strain. (c) Returning to 0% strain after 10 cycles with 60% uniaxial strain. (d) At 0% uniaxial strain without applying any strain. The arrows indicate the stretch direction.

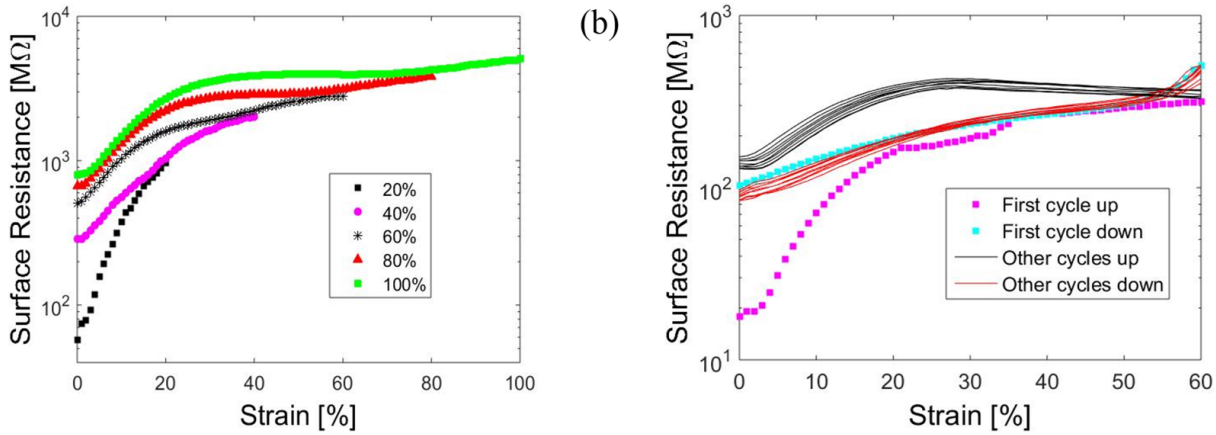

Fig. 6. Surface resistance vs. strain for MWCNT/P3DT monolayer transferred onto PDMS substrate (a) Starting with 20% strain up to 100% with 20% steps on the same sample and with a release to 0% after each stretch. (b) During 10 cycles with 60% uniaxial strain (30 s delay between each cycle).

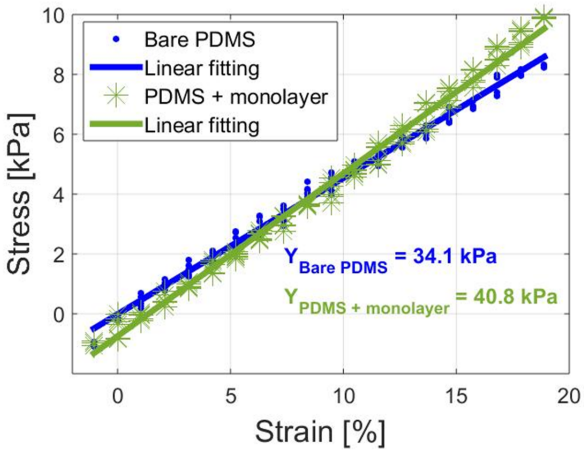

Fig. 7. Stress-strain curve of a bare PDMS substrate and of the same PDMS substrate covered with MWCNT/P3DT monolayer electrode, allowing the monolayer stiffness to be determined.

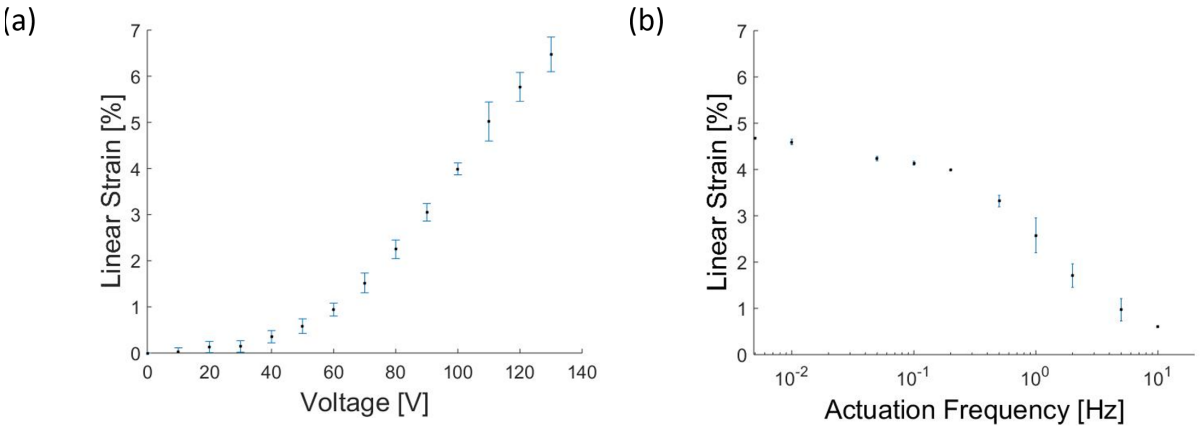

Fig. 8. Characterization of DEA consisting of a 1.4 µm thick silicone elastomer membrane with the monolayer electrodes. (a) Strain vs. voltage curve, showing over 5% linear strain at 100V. (b) Strain vs. actuation frequency curve.